Symbolic Time-Series Analysis for Anomaly Detection in Mechanical Systems

Amol Khatkhate, Asok Ray, *Fellow, IEEE*, Eric Keller, Shalabh Gupta, and Shin C. Chin

***Abstract*—This paper examines the efficacy of a novel method for anomaly detection in mechanical systems, which makes use of a hidden Markov model, derived from the time-series data of pertinent measurement(s). The core concept of the anomaly detection method is symbolic time-series analysis that is built upon the principles of *Automata Theory*, *Information Theory*, and *Pattern Recognition*. The performance of this method is compared with that of other existing pattern-recognition techniques from the perspective of early detection of small fatigue cracks in ductile alloy structures. The experimental apparatus, on which the anomaly detection method is tested, is a multi-degree-of-freedom mass-beam structure excited by oscillatory motion of two electromagnetic shakers. The evolution of fatigue crack damage at one or more failure sites are detected from symbolic time-series analysis of displacement sensor signals.**

***Index Terms*—Anomaly detection, fatigue crack damage, symbolic dynamics, time-series analysis.**

I. Introduction

An ANOMALY is defined as deviation from the nominal behavior of a dynamical system and is often associated with parametric and nonparametric changes that may gradually evolve in time. Anomalies may manifest themselves with self-excitation within the dynamical system, or under excitation of exogenous stimuli. On the sole basis of the fundamental principles of physics, the accurate and computationally tractable modeling of complex system dynamics is often infeasible; such a model may only exhibit the ensemble-averaged behavior of the physical process [1]. Therefore, it is necessary to rely on time-series data generated from sensors and other sources of information [2].

Several researchers [3]–[5] have addressed the problem of structural health monitoring based on time-series data. Along this line, a novel concept of anomaly detection has been proposed by Ray [6], where the underlying information on the dynamical behavior of complex systems is derived based on the following assumptions:

1) the process has stationary dynamics at the fast time scale;
2) any observable nonstationary behavior is associated with changes evolving at the slow time scale at which anomalies may occur.

Manuscript received July, 2004; revised April, 2006. Recommended by Technical Editor B. Yao. This work was supported in part by the U.S. Army Research Laboratory and the U.S. Army Research Office under Grant DAAD19-01-1-0646.

A. Khatkhate, A. Ray, E. Keller, and S. Gupta are with the Pennsylvania State University, University Park, PA 16802 USA (e-mail: amk303@psu.edu; axr2@psu.edu; eekeller@psu.edu; szg107@psu.edu).

S. C. Chin is with the U.S. Naval Research Laboratory, Washington, DC 20375 USA (e-mail: shin.chin@nrl.navy.mil).

Digital Object Identifier 10.1109/TMECH.2006.878544

The above-mentioned method of anomaly detection requires both temporal and spatial discretization of the pertinent measurement data to construct a sequence of symbols [7], [8]. The symbol sequence is treated as a transform of the original time-series data of measurements from the phase space into a symbol space such that no significant information is lost [9], [10]. This transform method is called symbolic time-series analysis in technical literature [2].

This paper makes use of symbolic time-series analysis for early detection of small anomalies, resulting from fatigue crack damage in ductile alloys, which is a major source of failures in structural components of operating machinery [11]. The objective is to capture this information from the observed time-series data as early as possible so that the decision and control system may take appropriate actions to avert catastrophic failures and satisfy the mission requirements albeit at a degraded level of performance [12].

The anomaly detection method is experimentally validated on a laboratory-scale test apparatus, where the source of possible anomalies is fatigue damage in vibrating mechanical structures. (Note that the evolution of fatigue damage is several orders of magnitude slower than the structural dynamics.) The test apparatus is designed to have sufficient complexity in itself due to partially correlated interactions amongst its individual components and functional modules [1]. Performance and efficacy of the proposed anomaly detection method has been assessed for detection of slowly evolving fatigue damage in the short-crack regime by comparison with other existing pattern recognition techniques, such as principal component analysis (PCA), multilayer perceptron neural networks (MLPNN), and radial basis function neural networks (RBFNN) [13]–[15].

The paper is organized into eight sections including the presentone. Section II briefly describes the test apparatus for experimental validation of anomaly detection. Section III discusses how fatigue crack damage evolves as an anomaly in the dynamical behavior of the test apparatus. Section IV briefly reviews the basic concepts of symbolic dynamics for anomaly detection in complex systems. Section V introduces the *D-Markov machine* method [6] for anomaly detection. Section VI presents existing pattern-recognition techniques that have relevance in the present context of anomaly detection. Section VII presents the experimental results and compares the *D-Markov machine* method with other existing pattern-recognition techniques from the perspective of early detection of small fatigue cracks in ductile alloys. Finally, the paper is summarized and concluded in Section VIII with recommendations for future research.

1083-4435/$20.00 © 2006 IEEE

Report Documentation Page

Form Approved
OMB No. 0704-0188

Public reporting burden for the collection of information is estimated to average 1 hour per response, including the time for reviewing instructions, searching existing data sources, gathering and maintaining the data needed, and completing and reviewing the collection of information. Send comments regarding this burden estimate or any other aspect of this collection of information, including suggestions for reducing this burden, to Washington Headquarters Services, Directorate for Information Operations and Reports, 1215 Jefferson Davis Highway, Suite 1204, Arlington VA 22202-4302. Respondents should be aware that notwithstanding any other provision of law, no person shall be subject to a penalty for failing to comply with a collection of information if it does not display a currently valid OMB control number.

1. REPORT DATE **APR 2006**	2. REPORT TYPE	3. DATES COVERED **00-00-2006 to 00-00-2006**
4. TITLE AND SUBTITLE **Symbolic Time-Series Analysis for ANomaly Detection in Mechanical Systems**		5a. CONTRACT NUMBER
		5b. GRANT NUMBER
		5c. PROGRAM ELEMENT NUMBER
6. AUTHOR(S)		5d. PROJECT NUMBER
		5e. TASK NUMBER
		5f. WORK UNIT NUMBER
7. PERFORMING ORGANIZATION NAME(S) AND ADDRESS(ES) **Pennsylvania State University,Mechanical Engineering Department,University Park,PA,16802**		8. PERFORMING ORGANIZATION REPORT NUMBER
9. SPONSORING/MONITORING AGENCY NAME(S) AND ADDRESS(ES)		10. SPONSOR/MONITOR'S ACRONYM(S)
		11. SPONSOR/MONITOR'S REPORT NUMBER(S)
12. DISTRIBUTION/AVAILABILITY STATEMENT **Approved for public release; distribution unlimited**		
13. SUPPLEMENTARY NOTES		
14. ABSTRACT **see report**		
15. SUBJECT TERMS		

16. SECURITY CLASSIFICATION OF:			17. LIMITATION OF ABSTRACT	18. NUMBER OF PAGES	19a. NAME OF RESPONSIBLE PERSON
a. REPORT **unclassified**	b. ABSTRACT **unclassified**	c. THIS PAGE **unclassified**	**Same as Report (SAR)**	**9**	

Standard Form 298 (Rev. 8-98)
Prescribed by ANSI Std Z39-18

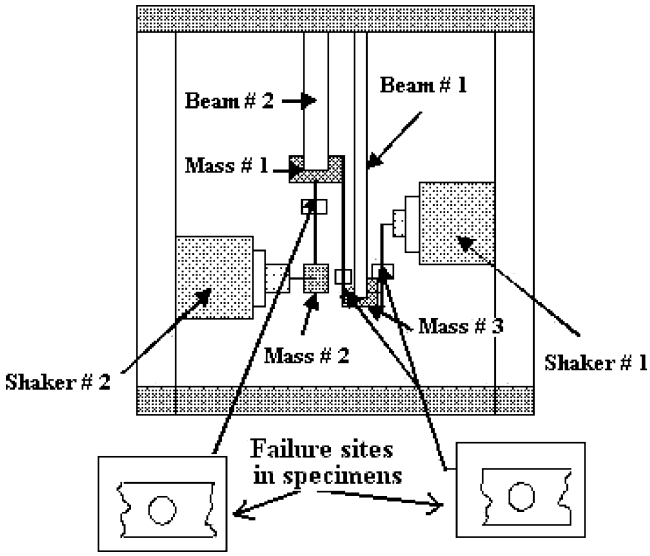

Fig. 1. Schematic diagram for the test apparatus.

TABLE I
STRUCTURAL DIMENSIONS OF THE TEST APPARATUS

Component	Material	Length (mm),Mass (kg) (Length x Width x Thickness)
Mass 1	Mild Steel	2.82
Mass 2	Aluminium 6061-T6	0.615
Mass 3	Mild Steel	3.87
Beam 1	Mild Steel	800 x 22 x 11
Beam 2	Aluminium 6061-T6	711.2 x 22.2 x 11.1
Specimens	Aluminium 6061-T6	203.2 x 22.2 x 11.1

II. DESCRIPTION OF THE TEST APPARATUS

The test apparatus is designed and fabricated as a multi-degree-of-freedom (DOF) mass-beam structure excited by oscillatory motion of two vibrators as shown in Fig. 1. Physical dimensions of the pertinent components are listed in Table I. Two of the three major DOFs are directly controlled by the two actuators, Shaker #1 and Shaker #2, and the remaining DOF is observable via displacement measurements of the three vibrating masses: Mass #1, Mass #2, and Mass #3. The inputs to the multivariable mechanical structure are the forces exerted by the two actuators; and the outputs to be controlled are the displacements of Mass #2 and Mass #3. The failure site in each specimen, attached to the respective mass is a circular hole (of radius 3.81 mm) as shown in Fig. 1. The test apparatus system is logically partitioned into two subsystems: 1) the plant subsystem consisting of the mechanical structure including the test specimens to undergo fatigue crack damage, actuators and sensors and 2) the instrumentation and control subsystem consisting of computers, data acquisition and processing, and communications hardware and software. Frequency of the reference signal is 11.39 Hz that is the resonating frequency associated with Mass #3 in the mechanical structure. The test specimens are thus excited by different levels of cyclic stress as two of the specimens are directly affected by the vibratory inputs while the remaining one is subjected to resulting stresses, thus functioning as a coupling between the two vibrating systems. In the present configuration, three test specimens are identically manufactured and their material is 6061-T6 aluminum alloy. Nevertheless, different materials can be selected for individual specimens that may also undergo different manufacturing procedures. Future research will allow different materials and manufacturing methods for individual specimens.

III. GENERATION OF FATIGUE CRACK ANOMALY

The mechanical system of the test apparatus in Fig. 1 is persistently excited near resonance so as to induce a stress level that causes fatigue failure to yield an average life of approximately 20 000 cycles having a total duration of about 32 min. There exists considerable scatter in the fatigue data, and variations have been seen in the actual observed life of the specimens tested at an identical stress level. The scatter results as a consequence of fatigue sensitivity to a number of test and material parameters including specimen fabrication and surface preparation, metallurgical variables, specimen alignment in the apparatus, mean stress, and test frequency [16]. These uncertainty factors were taken into consideration for design of the three failure sites as shown in Fig. 1.

The dynamical system attains stationary behavior, in the fast time scale of machine vibrations, under persistent excitation in the vicinity of the resonant frequency. The applied stress is dominantly flexural (i.e., bending) in nature and the amplitude of oscillations is symmetrical about the zero mean level, i.e., it is a reversed stress cycle [17]. Under such cyclic loading conditions, the specimens undergo fatigue cracking where the gross stress is elastic and plasticity is only localized. The fatigue damage occurs at a time scale that is (several order of magnitude) slow relative to the fast time scale dynamics of the vibratory motion and eventually leads to a catastrophic failure. Close observation indicates that fatigue failure develops in the following pattern: 1) the repeated cyclic stress causes incremental crystallographic slip and formation of persistent slip bands; 2) gradual reduction of ductility in the strain-hardened areas results in the formation of submicroscopic cracks; and 3) the notch effect of the submicroscopic cracks concentrates stresses until complete fracture occurs. Crack initiation may occur at a microscopic inclusion or at local site(s) of local stress concentration. In this experimental apparatus, the sites of stress concentration are localized by creating a hole in each of the three specimens. Since the mechanical structure of the test apparatus consists of beams and masses, the underlying dynamics can be approximated by a finite set of first-order coupled differential equations with parameters of damping and stiffness. The damping coefficients are very small and the stiffness constants very slowly change due to the evolving fatigue crack. The main objective of the work reported in this paper is to detect the slowly evolving anomaly (i.e., decrease in stiffness) at an early stage by observing time-series data of the available displacement measuring sensors. (Additional ultrasonic sensors will be installed at local crack sites in future for enhancement of anomaly detection.)

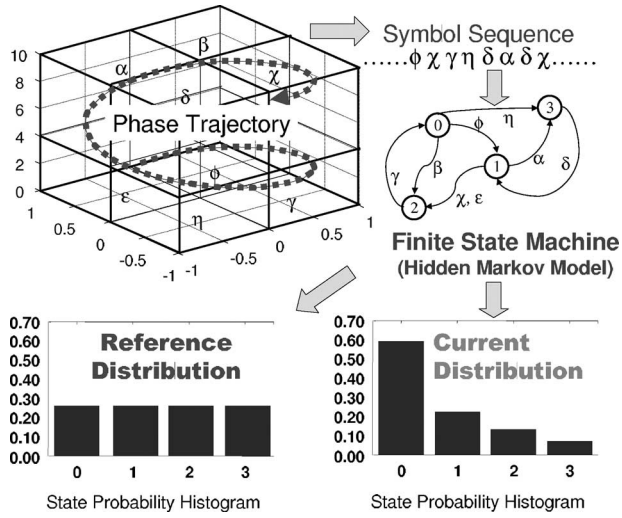

Fig. 2. Conceptual view of symbolic time-series analysis.

IV. Symbolic Dynamics and Encoding

The concept of *Symbolic Dynamics* and its usage for encoding nonlinear system dynamics from the observed time-series data have been reported in literature [2], [6]. It serves as a tool for behavior description of nonlinear dynamical systems based on the concept of *formal languages* for transitions from smooth dynamics to a discrete symbolic description [1], [6].

Fig. 2 elucidates partitioning of a compact (i.e., closed and bounded) region of the phase space and a mapping from the partitioned space into the symbol alphabet, which becomes a representation of the system dynamics defined by the trajectories. It also shows the construction of a hidden Markov model (HMM) from the symbol sequence as a finite-state machine. The quasi-stationary probability histograms of the states represent patterns that are indicative of the nominal (or reference) and anomalous behavior of the dynamical system, as explained in later sections.

Several methods of phase-space partitioning have been suggested in the literature [1], [18], [19]. One such method is symbolic false nearest neighbors (SFNN) [9] that finds a "generating" partition for symbolic orbits to uniquely identify a continuous-space orbit; thus, the symbolic dynamics become equivalent to the continuous-space dynamics. The key criterion for SFNN partitioning is that short sequences of consecutive symbols ought to localize the corresponding phase-space points as closely as possible. This is achieved by forming a particular geometrical embedding of the symbolic sequence under the candidate partition and minimizing the apparent errors in localizing phase-space points. The *nearest neighbor* to each point in the embedding is found in terms of Euclidean distance of symbolic neighbors. In general, better partitions yield a smaller proportion of SFNN. For convenience of implementation, the partitions are parameterized with a relatively small number of free parameters. This is accomplished by defining the partitions with respect to a set of radial-basis "influence" functions. The statistic for SFNN is minimized over these free parameters using genetic algorithms [9]. However, this partitioning method may become computationally very inefficient when the dimension of the phase space is large or if the data set is contaminated by noise.

This paper has adopted an alternative partitioning approach for construction of symbol sequences from the time-series data, which is particularly effective for noisy data from high-dimensional dynamical systems. In this method, called wavelet space (WS) partitioning [6], [10], the time-series data are first converted to the wavelet transform data at different scales and time shifts. The graphs of wavelet coefficients versus scale, at selected time shifts, are stacked starting with the smallest value of scale and ending with its largest value and then back from the largest value to the smallest value of the scale at the next instant of time shift. The arrangement of the resulting *scale series* data in the WS is then partitioned with alphabet size $|\mathcal{A}|$ by horizontal lines such that the regions with more information are partitioned finer and those with sparse information are partitioned coarser. In this approach, the maximum entropy is achieved by the partition that induces uniform probability distribution of the symbols in the symbol alphabet. Uniform probability distribution is a consequence of the maximum entropy partitioning.

V. D-Markov Machine Model

This section introduces the D-Markov machine model [6] for representing patterns in a symbolic process, which is motivated from the perspective of anomaly detection and is an alternative to the ε-machine [20]. The core concept of the D-Markov machine is succinctly presented below.

Let the symbolic representation of a discrete-time, discrete-valued stochastic process be denoted by: $\mathbb{S} \equiv \ldots S_{-2}S_{-1}S_0S_1S_2\ldots$. At any instant t, this sequence of random variables can be split into a sequence $\overleftarrow{S}_t$ of the past and a sequence $\overrightarrow{S}_t$ of the future. Assuming conditional stationarity of the symbolic process $\mathbb{S}$ (i.e., $P[\overrightarrow{S}_t|\overleftarrow{S}_t = \overleftarrow{s}]$ being independent of t), the subscript t can be dropped to denote the past and future sequences as $\overleftarrow{S}$ and $\overrightarrow{S}$, respectively. A symbol string, made of the first L symbols of $\overrightarrow{S}$, is denoted by $\overrightarrow{S}^L$. Similarly, a symbol string, made of the last L symbols of $\overleftarrow{S}$, is denoted by $\overleftarrow{S}^L$.

For $D \in \mathbb{N}$, the set of positive integers, a stochastic symbolic stationary process is called Dth-order Markov process if the probability of the next symbol depends only on the previous D symbols, i.e., the following condition holds:

$$P(s_i|s_{i-1}s_{i-2}\ldots) = P(s_i|s_{i-1}\ldots s_{i-D}). \tag{1}$$

Alternatively, symbol strings $\overleftarrow{S}, \overleftarrow{S}' \in \overleftarrow{\mathbf{S}}$ become indistinguishable whenever the respective substrings $\overleftarrow{S}^D$ and $\overleftarrow{S}'^D$, made of the most recent D symbols, are identical. Thus, a set $\{\overleftarrow{S}^L : L \geq D\}$ of symbol stings can be partitioned into a maximum of $|\mathcal{A}|^D$ equivalence classes [6], where $\mathcal{A}$ is the symbol alphabet. Each symbol string in $\{\overleftarrow{S}^L : L \geq D\}$, derived from a stationary process, belongs to exactly one of the $|\mathcal{A}|^D$ equivalence classes. Given $D \in \mathbb{N}$ and a symbol string $\overleftarrow{s}$ with $|\overleftarrow{s}| = D$, the *effective* state $q(D, \overleftarrow{s})$ is the equivalence class

of symbol strings defined as

$$q(D, \overleftarrow{s}) = \{\overleftarrow{S} \in \overleftarrow{\mathbf{S}} : \overleftarrow{S}^D = \overleftarrow{s}\} \tag{2}$$

and the set $\mathbf{Q}(D)$ of *effective* states of the symbolic process is the collection of all such equivalence classes. That is

$$\mathbf{Q}(D) = \{q(D, \overleftarrow{s}) : \overleftarrow{s} \in \overleftarrow{\mathbf{S}}^D\} \tag{3}$$

and hence $|\mathbf{Q}(D)| = |\mathcal{A}|^D$. A random variable for a state in the above set $\mathbf{Q}$ of states is denoted by $\mathcal{Q}$ and the jth state as q_j. The probability of transitions from state q_j to state q_k is defined as

$$\pi_{jk} = P(s \in \overrightarrow{S}^1 | q_j \in \mathbf{Q}, (s, q_j) \to q_k)$$
$$\sum_k \pi_{jk} = 1. \tag{4}$$

Given an initial state and the next symbol from the original process, only certain successor states are accessible. This is represented as the allowed state transitions resulting from a single symbol. Note that $\pi_{ij} = 0$ if $s_2 s_3 \ldots s_D \neq s'_1 \ldots s'_{D-1}$ whenever $q_i \equiv s_1 s_2 \ldots s_D$ and $q_j \equiv s'_1 s'_2 \ldots s'_D$. Thus, for a D-Markov machine, the stochastic matrix $\Pi \equiv [\pi_{ij}]$ becomes a branded matrix with at most $|\mathcal{A}|^{D+1}$ nonzero entries. The left eigenvector $\mathbf{p}$ corresponding to the unit eigenvalue of Π is the state probability vector under the (fast time scale) stationary condition of the dynamical system.

The construction of a D-Markov machine is fairly straightforward. Given $D \in \mathbb{N}$, the states are as defined in (2) and (3). On a given symbol sequence $\mathcal{S}$, a window of length $(D-1)$ is slided by keeping a count of occurrences of sequences $s_{i_1} \ldots s_{i_D} s_{i_{D+1}}$ and $s_{i_1} \ldots s_{i_D}$ which are respectively denoted by $N(s_{i_1} \ldots s_{i_D} s_{i_{D+1}})$ and $N(s_{i_1} \ldots s_{i_D})$. Note that if $N(s_{i_1} \ldots s_{i_D}) = 0$, then the state $q \equiv s_{i_1} \ldots s_{i_D} \in \mathbf{Q}$ has zero probability of occurrence. For $N(s_{i_1} \ldots s_{i_D}) \neq 0$, the transitions probabilities are then obtained by these frequency counts as follows:

$$\pi_{jk} = \frac{P(s_{i_1} \ldots s_{i_D} s)}{P(s_{i_1} \ldots s_{i_D})} \approx \frac{N(s_{i_1} \ldots s_{i_D} s)}{N(s_{i_1} \ldots s_{i_D})} \tag{5}$$

where the corresponding states are denoted by $q_j \equiv s_{i_1} s_{i_2} \ldots s_{i_D}$ and $q_k \equiv s_{i_2} \ldots s_{i_D} s$.

The time-series data under the nominal condition generates the state transition matrix Π^0 that, in turn, is used to obtain the probability vector $\mathbf{p}^0$, where $\mathbf{p}^0$ is the left eigenvector of Π^0 corresponding to the (unique) unit eigenvalue. Subsequently, probability vectors $\{\mathbf{p}^1, \mathbf{p}^2, \ldots\}$ are obtained at slow-time epochs $\{t_1, t_2, \ldots\}$ based on the respective time-series data. The behavioral changes from nominal condition are described as anomalies that are characterized by a scalar called *Anomaly Measure*$(\hat{\mathcal{M}})$. The anomaly measure is based on the following assumptions.

1) *Assumption 1:* The evolution of damage is an irreversible process, i.e., with zero probability of self healing. This assumption implies the following conditions for all time $t \geq 0$:
   a) $\hat{\mathcal{M}} \geq 0$;
   b) $\frac{d\hat{\mathcal{M}}}{dt} \geq 0$.
2) *Assumption 2:* The damage accumulation at a slow-time epoch t, when the dynamical system has reached a quasi-steady-state equilibrium, is a function of the entire path taken to reach that state.

Although the crack length is traditionally defined by a straight line joining the starting point to the tip of the crack, the actual crack follows a complicated path, possibly fractal in ductile materials, to reach a particular point. Therefore, assumption 2 implies that the anomaly measure should be determined from the actual path traversed and not just the end points. Accordingly, the path traversed also called the scalar-valued anomaly measure $\hat{\mathcal{M}}_k$ at a slow-time epoch t_k is defined in terms of a distance function $d(\cdot, \cdot)$ as

$$\hat{\mathcal{M}}_k \equiv \hat{\mathcal{M}}(t_k) \equiv \sum_{l=1}^{k} d\left(\mathbf{p}^l, \mathbf{p}^{l-1}\right) \tag{6}$$

$$d(\mathbf{x}, \mathbf{y}) = \left(\sum_{j=1}^{|\mathcal{A}|} |x_j - y_j|^\alpha\right)^{\frac{1}{\alpha}} \tag{7}$$

where the exponent $\alpha \in [1, \infty)$ depends on the desired sensitivity to small deviations. Small changes in the signal profile, which might be due to spurious fluctuations in the signal, can be suppressed with large values of α. Therefore, the choice of α is a tradeoff between suppression of small spurious fluctuations due to noise and those due to the actual changes in the signal profile resulting from damage growth. In this paper, the exponent is chosen to be $\alpha = 2.0$, which implies that $d(\cdot, \cdot)$ is the standard Euclidean distance. The distance traveled is calculated from the starting point ($\mathbf{p}^0 \equiv$ uniform distribution obtained with maximum entropy partitioning) to the current time epoch along the evolution of the probability vector (see Fig. 2).

VI. Existing Pattern-Recognition Techniques

This section briefly describes the following three pattern-recognition techniques, which use time-series data as inputs, for comparison with the symbolic-time-series-based anomaly detection method:

1) PCA;
2) MLPNN;
3) RBFNN.

While details of these methods are provided in a previous publication [15], they are briefly described in this paper for the sake of completeness.

A. PCA

Feature extraction methods in statistical pattern recognition determine an appropriate subspace of dimensionality $q \in \mathbb{N}$, where $\mathbb{N}$ is the set of positive integers, using either linear or nonlinear methods in the original feature space of dimensionality $n (q \leq n)$. The best-known linear feature extractor relies on the PCA or Karhunen–Loève expansion [13]. The eigenvectors of the $(n \times n)$ (positive semi-definite) covariance matrix of the time-series data, corresponding to the q largest eigenvalues, form the n-dimensional patterns. The linear transformation is defined as

$$Y = HX \tag{8}$$

where X is the given $(n \times d)$ pattern matrix, made of n row vectors; H is the $q \times n$ linear transformation matrix whose rows represent q feature vectors of dimension n; and Y is the derived $d \times q$ pattern matrix. Since the PCA method uses the most expressive features (e.g., eigenvectors with the largest eigenvalues), it effectively approximates the data by a linear subspace using the mean squared error criterion.

To detect growth in anomaly from time-series data, PCA is performed for dimensionality reduction. If the time response of an appropriate process variable $y(t)$ is sampled to generate a time-series sequence y_k, then data samples of large enough length $(\ell = dn)$ can be used to capture the dynamical characteristics of the observed process. The length ℓ of time-series data is partitioned into d subsections, each being of length $n = \ell/d$, where $d>n$. The resulting $(d \times n)$ data matrix is processed to generate the $(n \times n)$ covariance matrix that is positive-definite or positive-semidefinite real-symmetric. The next step is to compute the orthonormal eigenvectors $\mathbf{v}^1, \mathbf{v}^2, \ldots, \mathbf{v}^n$ and the corresponding eigenvalues $\lambda_1, \lambda_2, \ldots, \lambda_n$ that are arranged in decreasing orders of magnitude. The eigenvectors associated with the first (i.e., largest) q eigenvalues are chosen as the feature vectors such that

$$\frac{\sum_{i=q+1}^{n} \lambda_i}{\sum_{i=1}^{n} \lambda_i} < \eta \tag{9}$$

where the threshold $\eta \ll 1$ is a positive real close to 0. The resulting pattern is the matrix, consisting of the feature vectors as columns

$$\widetilde{M} = \left(\sqrt{\lambda_1}\mathbf{v}_1 \cdots \sqrt{\lambda_q}\mathbf{v}_q\right). \tag{10}$$

The above steps are executed for time-series data under the nominal (stationary) condition to obtain $\widetilde{M}_0$. Then, these steps are repeated at subsequent slow-time epochs $\{t_1, t_2, \ldots\}$ as the (possible) anomaly progresses using the same values of parameters ℓ, d, n, and q, used under the nominal condition, to obtain the respective pattern matrices $\widetilde{M}_1, \widetilde{M}_2, \ldots$. The anomaly measures at slow-time epochs $\{t_1, t_2, \ldots\}$ are obtained as

$$\hat{\mathcal{M}}_k \equiv d\left(\widetilde{M}_k, \widetilde{M}_0\right)$$

where $d(\cdot,\cdot)$ is an appropriately defined path-dependent distance function as given by (6).

It should be noted that different metrics may be used as anomaly measures as stated in [6]. One may choose the metric that yields the most satisfactory result for the specified purpose. Along this line, different metrics could be chosen for other pattern-recognition techniques.

B. MLPNN for Anomaly Detection

The MLPNN is the most commonly used family of feed-forward neural networks for pattern classification tasks [13]. The MLPNN is a collection of connected processing elements called nodes or neurons [14], [21]. Its structure is fixed by choosing the number of layers as well as the (possibly different) number of neurons in each layer. The MLPNN is trained based on the information contained in a given set of inputs and target outputs. The *training* phase includes modeling of the input–output system architecture and identification of the synapsis weights. A set of inputs is passed forward through the network, yielding trial outputs that are then compared to the target outputs to obtain the error (i.e., the deviation of the trial output from the target output). The network parameters (i.e., synapsis weights and biases) are adjusted until the error is within specified limits. If the specified bound is exceeded, the error is passed *backwards* through the net and the *training algorithm* adjusts the synapsis weights.

The *back-propagation* algorithm has been used in this paper. The simplest implementation of back-propagation learning updates the network weights and biases in the direction in which the performance function decreases most rapidly. The *mean square error* criterion is adopted in the recursive algorithm to update the weight vectors $\{w_k\}$ as follows:

$$\mathbf{w}_{n+1} = \mathbf{w}_n - \alpha_n \mathbf{g}_n \tag{11}$$

where $\mathbf{g}_n$ is the gradient and α_n is the learning rate.

Different layers in MLPNN may contain different numbers of neurons. Time-series signals enter into the input layer nodes, progress forward through the hidden layers, and finally emerge from the output layer. Each node i at a given layer k receives a signal from all nodes j in its preceding layer $(k-1)$ through a synapsis of weight w_{ij}^k and the process is carried onto the nodes in the following layer $(k+1)$. The weighted sum of signals x_j^{k-1} from all nodes j of the layer $(k-1)$ together with a bias w_{i0}^k produces the excitation z_i^k that, in turn, is passed through a nonlinear *activation function f* to generate the output x_i^k from the node i at layer k. This is mathematically expressed as

$$z_i^k = \sum_j w_{ij}^k x_j^{k-1} + w_{i0}^k \tag{12}$$

$$x_i^k = f\left(z_i^k\right). \tag{13}$$

Various choices for the activation function f are possible; the hyperbolic tangent function $f(x) = \tanh(x)$ has been adopted in this paper.

For anomaly detection, the MLPNN is trained by setting a set of N input vectors, each of dimension ℓ, and a specified target output vector τ of dimension q. This implies that the input layer has ℓ neurons and the output layer has q neurons. If the time-series data are obtained from an ergodic process, then a data set of length $N.\ell$ can be segmented into N vectors of length ℓ to construct the input and target pattern matrices, $\mathcal{P}$. The input pattern matrix $\mathcal{P} \in \mathbb{R}^{\ell \times N}$ is obtained from the N input vectors as

$$\mathcal{P} \equiv [\mathbf{p}^1 \mathbf{p}^2 \cdots \mathbf{p}^N] \tag{14}$$

where $\mathbf{p}^k \equiv [y_{(k-1)\ell+1} y_{(k-1)\ell+2} \ldots y_{k\ell}]^T$ and each y_k is a sample from the ensemble of the time-series data. The corresponding output matrix $\mathcal{O}$ is the output of the trained MLPNN under the input pattern $\mathcal{P}$

$$\mathcal{O} \equiv \left[\mathbf{o}^1 \mathbf{o}^2 \cdots \mathbf{o}^N\right] \tag{15}$$

where $\mathbf{o}^i \in \mathbb{R}^q$ is the output of the trained MLPNN under the input $\mathbf{p}^k \in \mathbb{R}^\ell$. The performance vector $\mathbf{u} \in \mathbb{R}^q$ is obtained as

the average of the N outputs

$$\mathbf{u} \equiv \frac{1}{N}\sum_{k=1}^{N}\mathbf{o}^k. \tag{16}$$

The time-series data under the nominal condition generates the input pattern matrix $\mathcal{P}_0$ that, in turn, is used to train the MLPNN with respect to a target output vector τ. The resulting output of the trained MLPNN with $\mathcal{P}_0$ as the input is $\mathcal{O}_0$ and the performance vector is $\mathbf{u}_0$. Subsequently, input pattern matrices $\{\mathcal{P}_1, \mathcal{P}_2, \ldots\}$ are obtained at slow-time epochs $\{t_1, t_2, \ldots\}$ and corresponding output matrices of the trained MLPNN are $\{\mathcal{O}_1, \mathcal{O}_2, \ldots\}$, which yield the respective performance vectors $\{\mathbf{u}_1, \mathbf{u}_2, \ldots\}$. The anomaly measures at slow-time epochs $\{t_1, t_2, \ldots\}$ are obtained as

$$\hat{\mathcal{M}}_k \equiv d(\mathbf{u}_k, \mathbf{u}_0)$$

where $d(\cdot,\cdot)$ is an appropriately defined path-dependent distance function as given by (6).

C. RBFNN for Anomaly Detection

The RBFNN is a commonly used tool for pattern identification [14], where the activation of a hidden unit is determined by the distance between the input vector and the prototype vector; the RBFNN is essentially a nearest-neighbor type of classifier. A radial basis function has the following structure:

$$f(y,\alpha) = \exp\left(-\frac{\sum_k |y_k - \mu|^\alpha}{N\theta_\alpha}\right) \tag{17}$$

where the exponent parameter $\alpha \in (0,\infty)$; and μ and θ_α are the center and αth central moment of the data set, respectively. For $\alpha = 2$, $f(\cdot)$ becomes Gaussian, which is the typical radial basis function used in the neural network literature. To perform anomaly detection, the first task is to obtain the sampled time-series data when the dynamical system is in the nominal condition and then the mean μ and the central moment θ_α are calculated as

$$\mu = \frac{1}{N}\sum_{k=1}^{N} y_k \quad \text{and} \quad \theta_\alpha = \frac{1}{N}\sum_{k=1}^{N}|y_k - \mu|^\alpha. \tag{18}$$

The distance between any vector y and the center μ is obtained as $d(y,\mu) \equiv (\sum_n |y(n) - \mu|^\alpha)^{\frac{1}{\alpha}}$. Following (17), the radial basis function at the nominal condition is $f_0 = f(y)$. Under all conditions including anomalous ones, the parameters μ and θ are kept fixed. However, at slow-time epochs $\{t_1, t_2, \ldots\}$, the radial basis functions $\{f_1, f_2, \ldots\}$ are evaluated from the data sets under the (possibly anomalous) conditions. The anomaly measure at the epoch t_k in the slow time scale is obtained as a distance from the nominal condition and is given by

$$\hat{\mathcal{M}}_k = d(f_0, f_k)$$

where $d(\cdot,\cdot)$ is an appropriately defined path-dependent distance function as given by (6).

VII. Experimental Validation

This section makes a comparative assessment of the D-Markov machine method with different pattern-recognition techniques for anomaly detection. Time-series data, generated from experiments on the test apparatus in Fig. 1, have been used for this purpose. Both the vibrators in the test apparatus were excited by a sinusoidal input of amplitude 0.85 V and frequency 11.39 Hz (approximately the resonance frequency) throughout the run of each experiment. The time-series data of the displacement sensor on Mass #3, which serve as an indicator of the system performance, were collected from the beginning of the experiments until breakage of specimens. The ensemble of data were saved in a total of 35 files, with each file containing a minute of sensor time-series data. Following the procedure outlined in Sections IV–VI, the anomaly measure was obtained from the data at each 2-min interval from the sensor data contained in each file. The time-series data sets were collected after the dynamic response attained the stationary behavior. The data set at the time epoch of 2 min was taken as the reference point representing the nominal behavior of the dynamical system. These data sets were used to compare the anomaly detection capability of the symbolic dynamics approach relative to that of two existing pattern-recognition techniques: PCA and Neural Network. Since symbol generation from the time-series data is the crucial step in symbolic-dynamics-based anomaly detection, this paper investigates two alternative approaches—SFNN partitioning and WS partitioning.

The following anomaly detection approaches are investigated by using the same set of time-series data generated from the experiments on the test apparatus in Fig. 1:

1) PCA;
2) MLPNN;
3) RBFNN;
4) D-Markov machine with SFNN partitioning;
5) D-Markov machine with WS partitioning.

The description of how anomaly measures are calculated based on the above five techniques of pattern recognition is given later. The fourth paragraph addresses both SFNN and WS methods of partitioning in the D-Markov method.

Following the PCA procedure described in Section VI-A, a block of sampled time-series data, having length $\ell = 12\,000$, is divided into $n = 4$ segments of length $d = 3000$; these segments are arranged to form a 3000×4 data matrix. The resulting 4×4 (symmetric positive-definite) covariance matrix of the data matrix yields a monotonically decreasing set of eigenvalues, $\lambda_1 \ldots \lambda_4$, and the associated orthonormal eigenvectors $\mathbf{v}^1, \ldots, \mathbf{v}^4$. At the nominal condition, three eigenvalues are found to be dominant (i.e., $q = 3$) for a threshold of $\eta = 1.0 \times 10^{-3}$ such that

$$\frac{\sum_{i=3}^{4}\lambda_i}{\sum_{i=1}^{4}\lambda_i} = 0.0001 < \eta.$$

The matrix $\widetilde{M}_0$ in (10) is calculated from the data set at the nominal condition. Similarly, the matrices $\tilde{M}_2, \tilde{M}_4, \ldots, \tilde{M}_{32}$ are obtained corresponding to different time epochs, respectively. The anomaly measures at different time epochs are determined according to (6) relative to nominal matrix $\widetilde{M}_0$.

Following the MLPNN procedure described in Section VI-B, the resulting pattern matrix $\mathcal{P}_0$ is made of $N = 100$ columns.

Each column, having a length $\ell = 25$, is generated from the time-series data at nominal condition to train the MLPNN that is chosen to have a input layer (with 30 neurons), four hidden layers (with 50 neurons in layer 1, 40 neurons in layer 2, 30 neurons in layer 3, and 40 neurons in layer 4), and the output layer (with 5 neurons). This structure of the MLPNN yields very good convergence for the data sets under consideration. The target corresponding to each input pattern vector is chosen to be 5×1 zero vector. The MLPNN is trained with the nominal data set and the gradient descent back-propagation algorithm has been used for network training with an allowable performance mean square error of 1.0×10^{-5}. The input pattern matrices, $\mathcal{P}_0, \mathcal{P}_2, \mathcal{P}_4, \ldots, \mathcal{P}_{32}$, each of dimension (25×100), are then generated from the anomalous data sets at various time epochs to excite the trained network. The resulting output matrices of the trained MLPNN are $\mathcal{O}_0, \mathcal{O}_2, \mathcal{O}_4, \ldots, \mathcal{O}_{32}$, which yield the respective performance vectors, $\mathbf{u}_0, \mathbf{u}_2, \mathbf{u}_4, \ldots, \mathbf{u}_{32}$. The anomaly measures at different time epochs are determined according to (6).

Following the RBFNN procedure described in Section VI-C, the length of the sampled time-series data is chosen to be $N = 12\,000$. The exponent α for standard RBF is usually chosen to be 2, for improved anomaly measure sensitivity. An estimate of the parameters μ and θ_α are obtained according to (18) based on the data under the nominal condition, which yields the requisite radial basis function f_0 following (17). The anomaly measures at different time epochs are determined according to (6).

Based on the time-series data of the nominal condition, the first step in the D-Markov machine method is to find a partition for symbol sequence generation. The partitioning methods, SFNN and WS, described in Section IV, have been investigated for efficacy of anomaly detection. For the given stimulus of this experiment, partitioning of the phase space/WS must remain invariant at all epochs of the slow time scale. Absolute values of the wavelet scale series data (see Section IV) were used to generate the partition because of the symmetry of the data sets about their mean. The finite-state machine constructed with the choice of the parameters $|\mathcal{A}| = 8$ and $D = 1$ has only eight states and it was able to capture early anomalies. Increasing the value of $|\mathcal{A}|$ further did not improve the results and increasing the value of depth D created a large number of states of the finite-state machine, many of them having very small or zero probabilities. Hence, the value of $D = 1$ was used for construction of the D-Markov machine for data at all time epochs. Following the procedure described in Section V, the state machines are constructed to generate the connection matrix $\Pi \equiv [\pi_{jk}]$ and the state probability vector $\mathbf{p}$ for each slow time epoch. The state machines were constructed with a symbol alphabet of cardinality 8.

A. Comparison of Anomaly Detection Methods

The anomaly detection method is validated on the laboratory test apparatus in Fig. 1. Test runs are planned for exogenous stimuli at one of the natural frequencies of the mechanical structure to cause fatigue failure within reasonable length of time. Using the same set of time-series data generated from the above experiments, the five plots in Fig. 3 compare the anomaly measures obtained by using the aforementioned five anomaly detection approaches WS, SFNN, PCA, MLPNN, and RBFNN, for the first 16 files (i.e., up to ~32 min) when the service life of the test specimen has expired, i.e., the specimen is about to break. (Note: The estimated service life of the specimen under this load excitation is ~30 min.) The nominal condition is chosen at the time epoch of 2 min to ensure that all transients have decayed. Each of the five methods shows a sharp rise in the anomaly measure at about 22 min, which is indicative of the transition from the crack-incubation to the crack-propagation phase in fatigue damage. The symbolic time-series-based anomaly detection with both WS and SFNN give better performance than the three other existing pattern-recognition tools and are responsive to progressive damage in the short-crack regime till the time epoch of ~22 min. At this time, cracks begin to form, indicating the transition from crack incubation to crack initiation.

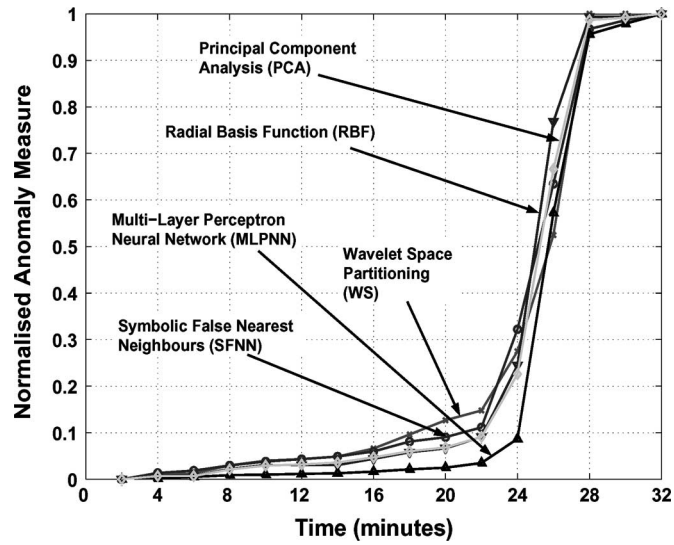

Fig. 3. Performance comparison of anomaly detection methods.

Physical modeling of fatigue damage in the short crack region has not been dealt with significantly in technical literature. Fig. 3 shows that symbolic time-series analysis under both WS and SFNN partitioning is able to capture the progressive accumulation of fatigue damage in the crack-initiation phase while the performance of PCA and RBFNN is somewhat inferior and MLPNN is the worst. This is indicated by the magnitude of the anomaly measure as well as the change in slope starting at ~15 min. Slope of the anomaly measure curve is representative of the rate of damage progression. The distributed nonlinearities in MLPNN may not be specifically suited to capture these small parameter perturbations in the largely linear behavior of the dynamic response of the vibrating structures. The WS partitioning shows higher anomaly measure as compared to PCA. The rationale is that the PCA method is dependent on eigenvalues and eigenvectors of the covariance matrix that is sensitive to measurement noise in the data acquisition process. In contrast, the symbolic time-series analysis, with both

WS and SFNN partitioning, is much less sensitive to (zero-mean) measurement noise because of the inherent averaging due to repeated path traversing in the finite-state machine. All five anomaly detection methods exhibit a gradual increase in anomaly measure from the beginning up to the time epoch of ~22 min, when the transition takes place from the short- to the long-crack regime. RBFNN, MLPNN, and PCA exhibit good performance in the long-crack regime in the 24–28-min interval. The specimen breaks at ~28 min.

VIII. Summary, Conclusion, and Future Work

This paper experimentally validates a novel tool using WS partitioning [6], [10] for the detection of evolving anomalies in dynamical systems and compares it with existing pattern-recognition techniques: PCA, MLPNN, and RBFNN. It is assumed that the unforced dynamical system (i.e., in the absence of external stimuli) is stationary at the fast time scale and that any nonstationary behavior is observable only on the slow time scale. Then, an HMM [6], [22], is constructed from the symbol sequences in the form of a probabilistic finite-state automaton. Anomaly measures at different slow-time epochs are obtained in real time as the distance between the state probability distribution at that epoch and the state probability distribution at the nominal condition incorporating the path traversed by the state probability vector. In this way, the anomaly measure quantifies damage growth relative to the nominal condition.

The following observations are made from the analysis of experimental data.

1) The results of symbolic time-series analysis on the laboratory apparatus show that the evolution of fatigue crack damage is detected in advance of component failure. This is of paramount importance to health and usage monitoring of machinery operations as it provides ample time to take remedial control actions for life extension [12] and reliability enhancement.
2) The symbolic time-series analysis, with WS and SFNN partitioning, is more effective for the detection of evolving anomalies in the crack initiation regime than the PCA, MLPNN, and RBFNN methods.

A major conclusion, based on this specific experimental investigation, is that symbolic time series, along with the stimulus–response methodology and having a vector representation of anomaly, is effective for the detection of small anomalies due to fatigue damage in ductile alloy materials.

Further theoretical and experimental research is recommended in the following areas:

1) theoretical research, supported by experimental validation, in phase-space and wavelet-space partitioning for generation of symbol sequences from time-series data;
2) validation of the symbolic time-series method for the detection of fatigue damage in different materials with various geometries and loading conditions;
3) understanding deeper aspects of fatigue crack initiation using advanced sensing technology such as ultrasonics and electromagnetics.

References

[1] R. Badii and A. Politi, *Complexity Hierarchical Structures and Scaling in Physics*. Cambridge, U.K.: Cambridge Univ. Press, 1997.

[2] C. Daw, C. Finney, and E. Tracy, "A review of symbolic analysis of experimental data," *Rev. Sci. Instrum.*, vol. 74, no. 2, pp. 915–930, 2003.

[3] S. W. Doebling, C. R. Farrar, M. B. Prime, and D. W. Shevitz, "Damage identification and health monitoring of structural and mechanical systems from changes in their vibration characteristics: A literature review," Los Alamos Nat. Lab. Tech.Rep. LA-13070-MS, 1996.

[4] Z. Peng and F. Chu, "Application of the wavelet transform in machine condition monitoring and fault diagnosis: A review with bibliography," *Mech. Syst. Signal Process.*, vol. 18, pp. 199–221, 2004.

[5] X. Lou and K. Loparo, "Bearing fault diagnosis based on wavelet transform and fuzzy interference," *Mech. Syst. Signal Process.*, vol. 18, pp. 1077–1095, 2004.

[6] A. Ray, "Symbolic dynamic analysis of complex systems for anomaly detection," *Signal Process.*, vol. 84, no. 7, pp. 1115–1130, 2004.

[7] C. Beck and F. Schlögl, *Thermodynamics of Chaotic Systems: An Introduction*. Cambridge, U.K.: Cambridge Univ. Press, 1993.

[8] D. Lind and M. Marcus, *A Introduction to Symbolic Dynamics and Coding*. Cambridge, U.K.: Cambridge Univ. Press, 1995.

[9] M. Kennel and M. Buhl, "Estimating good discrete partitions from observed data: Symbolic false nearest neighbors," *Phys. Rev. E*, vol. 91, no. 8, p. 084102, 2003.

[10] V. Rajagopalan and A. Ray, "Symbolic time series analysis via wavelet-based partitioning," *Signal Processing*, *in press* [Online]. Available: www.sciencedirect.com

[11] S. Ozekici, *Reliability and Maintenance of Complex Systems*, vol. 154. Berlin, Germany: NATO Advanced Science Institutes (ASI) Series F: Computer and Systems Sciences, 1996.

[12] H. Zhang, A. Ray, and S. Phoha, "Hybrid life extending control of mechanical systems: Experimental validation of the concept," *Automatica*, vol. 36, no. 1, pp. 23–36, 2000.

[13] R. Duda, P. Hart, and D. Stork, *Pattern Classification*. Hoboken, NJ: Wiley, 2001.

[14] C. M. Bishop, *Neural Networks for Pattern Recognition*. New York: Oxford Univ. Press, 1995.

[15] S. Chin, A. Ray, and V. Rajagopalan, "Symbolic time series analysis for anomaly detection: A comparative evaluation," *Signal Process.*, vol. 85, no. 9, pp. 1859–1868, 2005.

[16] A. Ray, "Stochastic measure of fatigue crack damage for health monitoring of ductile alloy structures," *Struct. Health Monit.*, vol. 3, no. 3, pp. 245–263, 2004.

[17] M. Klesnil and P. Lukas. (1992). *Fatigue of Metallic Materials Mater. Sci. Monographs*, vol. 71, New York: Elsevier.

[18] H. Abarbanel, *The Analysis of Observed Chaotic Data*. New York: Springer-Verlag, 1996.

[19] H. Kantz and T. Schreiber, *Nonlinear Time Series Analysis*, 2nd ed. Cambridge, U.K.: Cambridge Univ. Press, 2003.

[20] J. P. Crutchfield and K. Young, "Inferring statistical complexity," *Phys. Rev. Lett.*, vol. 63, pp. 105–108, 1989.

[21] M. Markou and S. Singh, "Novelty detection: A review—Parts 1 and 2," *Signal Process.*, vol. 83, pp. 2481–2521, 2003.

[22] L. Rabiner, "A tutorial on hidden Markov models and selected applications in speech processing," *Proc. IEEE*, vol. 77, no. 2, pp. 257–286, Feb. 1989.

Amol Khatkhate received the B.E. degree in mechanical engineering from Veer Mata Jijabai Technological Institute, Mumbai, India, in 2001. He received two M.S. degrees, one in mechanical engineering and the other in electrical engineering, both from the Pennsylvania State University (PSU), University Park. He is working toward the Ph.D. degree in mechanical engineering and also working as a Graduate Research Assistant at the Electromechanical Systems Laboratory, PSU.

His current research interests include diagnostics, and prognostics and structural health monitoring. His other research interests include control theory, signal processing, and pattern recognition.

Asok Ray (F'02) received graduate degrees in electrical engineering in 1970, mathematics in 1978, computer science in 1972, and the Ph.D. degree in mechanical engineering from Northeastern University, Boston, MA, in 1976.

In July 1985, he joined the Pennsylvania State University, University Park, and is currently a Distinguished Professor of Mechanical Engineering. His research interests include control and optimization of continuously varying and discrete-event dynamical systems, intelligent instrumentation for real-time distributed systems, and modeling and analysis of complex dynamical systems from thermodynamic perspectives.

Dr. Ray is a Fellow of ASME, a Fellow of World Innovation foundation, and an Associate Fellow of AIAA.

Eric Keller received the B.S. degree in mechanical engineering from Virginia Tech, Blacksburg, in 1982, the M.S. degree in aerospace engineering from the Air Force Institute of Technology, Wright Patterson Air Force Base, OH, in 1985, and the Ph.D. degree in mechanical engineering from the Pennsylvania State University (PSU), University Park, in 2001.

He has been a Senior Research Associate at the Applied Research Laboratory, PSU, since June 2001. His research interests include sensor networks, robotics, signal processing, and health monitoring systems. He was an Officer in the U.S. Air Force, from 1983 to 1994.

Shalabh Gupta received the B.Tech. (Honors) degree in mechanical engineering from the Indian Institute of Technology, Roorkee, India, in 2001. He received two M.S. degrees, one in mechanical engineering and the other in electrical engineering, both from the Pennsylvania State University (PSU), University Park. Currently, he is working toward the Ph.D. degree in mechanical engineering at the PSU.

His current research interests include control theory, signal processing, pattern recognition, fault diagnosis, and statistical mechanics.

Shin C. Chin received the B.Sc. degree in electrical engineering from the University of Michigan, Ann Arbor, in 1992. He received two M.Sc. degrees, one in physics, and the other in electrical engineering, in 1994 and 1998, respectively, both from the University of Michigan. He received the Ph.D. degree in electrical engineering from the Pennsylvania State University (PSU), University Park, in 2004.

He is currently with the Naval Research Laboratory, Washington, DC. His research interests include signal and image processing and pattern recognition.